Electromagnetic Biology and Medicine, 26: 239–250, 2007

ISSN 1536-8378 print
DOI: 10.1080/15368370701572712

informa
healthcare

Modeling Environment for Numerical Simulation of Applied Electric Fields on Biological Cells

DANIELA OTA HISAYASU SUZUKI[1],
AIRTON RAMOS[2], AND
JEFFERSON LUIZ BRUM MARQUES[1]

[1]Department of Electrical Engineering, Institute of Biomedical Engineering, Federal University of Santa Catarina (UFSC), Santa Catarina, Brazil
[2]Electrical Engineering Department, Centre of Technological Sciences, State University of Santa Catarina (UDESC), Santa Catarina, Brazil

The application of electric pulses in cells increases membrane permeability. This phenomenon is called electroporation. Current electroporation models do not explain all experimental findings: part of this problem is due to the limitations of numerical methods. The Equivalent Circuit Method (ECM) was developed in an attempt to solve electromagnetic problems in inhomogeneous and anisotropic media. ECM is based on modeling of the electrical transport properties of the medium by lumped circuit elements as capacitance, conductance, and current sources, representing the displacement, drift, and diffusion current, respectively. The purpose of the present study was to implement a 2-D cell Model Development Environment (MDE) of ionic transport process, local anisotropy around cell membranes, biological interfaces, and the dispersive behaviour of tissues. We present simulations of a single cell, skeletal muscle, and polygonal cell arrangement. Simulation of polygonal form indicates that the potential distribution depends on the geometrical form of cell. The results demonstrate the importance of the potential distributions in biological cells to provide strong evidences for the understanding of electroporation.

Keywords Bioelectromagnetism; Biological effects of electromagnetic fields; Biological system modeling; Field calculation.

Introduction

Eletropermeabilization or electroporation is the phenomenon in which the cell membrane exposed to an electric field became permeable to ions and molecules

Address correspondence to Jefferson Luiz Brum Marques, Department of Electrical Engineering, Institute of Biomedical Engineering, Federal University of Santa Catarina, Campus Universitário, Trindade, Florianópolis, SC 88040-900, Brazil; E-mail: jmarques@ieb.ufsc.br

(Kinosita and Tsong, 1977). This method is used to insert proteins, DNA, and drugs into living cells (Neumann et al., 2000). The electroporation of cells is employed in biotechnology, genetics, and treatment of head and neck cancer (Hoffmann et al., 1996).

Electrochemotherapy is the treatment of solid tumors which combines chemotherapic drugs, like bleomycin, with electropermeabilization of plasmatic membranes (Mir and Orlowski, 1999). However, eletropermeabilization depends on short and intense electric pulses and the biological medium as well. For a safe treatment it is important to understand the electrical characteristics of tissues and the eletropermeabilization.

Unfortunately, none of the electroporation models explain all experimental results (Abidor et al., 1979; Glaser et al., 1988; Weaver and Mintzer, 1981). We believe that this gap is partly due to the limitations of usual numerical methods for computing electromagnetic fields in biological materials and cell suspensions, such as finite difference method (FDM) (Valencic et al., 1994) and finite element method (FEM) (Semrov and Miklavcic, 2000).

The Equivalent Circuit Method (ECM) was developed in an attempt to solve electromagnetic problems in inhomogeneous and anisotropic media, like the biological medium (Ramos et al., 2003). ECM is based on modeling of the electrical transport properties of the medium by lumped circuit elements as capacitance, conductance, and current sources, representing the displacement, drift, and diffusion current, respectively.

The aim of this study was to implement a 2-D cell Model Development Environment (MDE) of the ionic transport process, local anisotropy around cell membranes, and biological interfaces and the dispersive behavior of tissues.

Materials and Methods

Equivalent Circuit Method—Cell Scale Model

Initially, the volume under analysis should be divided into a large number of small rectangular parallelepiped shown in Fig. 1. Each block constitutes a node of

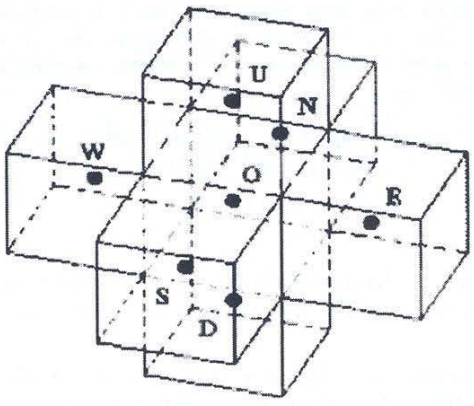

Figure 1. Space discretization in a parallelepiped mesh.

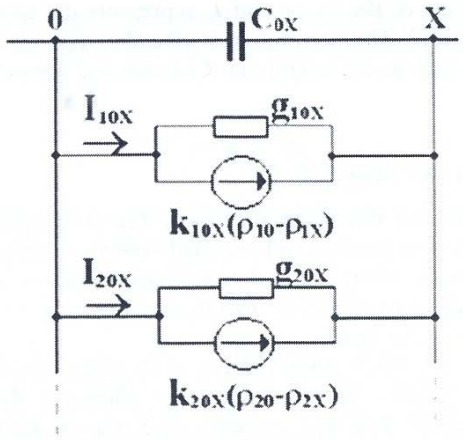

Figure 2. Equivalent circuit for cell scale model. The letters O and X indicate nodes of circuit. The numbers 1 and 2 indicate different charge carrier types.

equivalent circuit and communicates with its neighbors by a set of paralleled circuit proposed in Fig. 2. Each element of the equivalent circuit is calculated based on the dimensions of the block and the local electric and transport properties in that point of the space. So, the total current leaving each node of the circuit is given by the following difference equation:

$$I = \sum_i \sum_n (g_{ni}\Delta_i V + k_{ni}\Delta_i \rho_n) + \sum_i C_i \frac{\delta(\Delta_i V)}{\delta t} \tag{1}$$

where the summation is extended over all 'n' different charge carriers presented in the medium and over the three directions of the space ($i = x, y, z$). V and ρ are the electric potential and charge density inside a block. Δ and δ indicate difference in space and time. The parameters g, k, and C are the conductance, diffusion coefficient, and capacitance of the block, respectively, and they are given by:

$$g_{ni} = \rho_n \mu_{ni} \frac{A_i}{L_i}, \quad k_{ni} = f_n D_{ni} \frac{A_i}{L_i}, \quad C_i = \varepsilon_i \frac{A_i}{L_i}, \tag{2}$$

where μ_n and D_n are the mobility and diffusion coefficients of the charge carrier n and ε is the permittivity of the medium. A and L are the area and length of the connection between two blocks and f_n is a voltage-dependent factor from the solution of the one-dimensional Nernst–Planck equation between the two nodes.

Electric potential and charge distributions are obtained by solving the resulting electric circuit in the time domain for given boundary and initial conditions (Ramos et al., 2003). The charge densities for each charger carrier have to be updated at each time step according to:

$$\rho_n^{\text{actual}} = \rho_n^{\text{former}} - \frac{1}{\Delta v} \sum I_{qn}^{\text{former}} \Delta t \tag{3}$$

where Δv is the volume of the block and I_q represents the total charge movement current (drift + diffusion). The summation is extended over all branches connecting the node considered and its six neighbors. Currents are considered positives when leaving the node.

Length Discretization and Time Step

Length discretization and time step determine the convergence of the iterative process. The discretization problem in biological systems is about the cell membrane and biological interfaces, where we find charge accumulation and field variations. The cells are very close to each other, therefore using only a few blocks or nodes will cause distortions in the results.

The first step in the MCE discretization is to define the regular mesh, either rectangle or square blocks. We use this mesh whenever there are only small variations on the electric field and currents. The discretization in Fig. 3(b) uses 16×16 divisions. The distortions are showed circles, highlighting an inexistent contact point between cells. Figure 3(c) has a 64×64 grid. The distortions were reduced, but both the number of nodes and the computational time have increased. The best solution achieved was to define a high resolution area in the regular mesh that solves the discretization problem. Within the high resolution areas, the number of nodes is multiplied by a factor named "node multiplier" (user specified). The resulting regular mesh with high resolution areas is showed in Fig. 3(d): the node multiplier factor is four and the number of nodes is smaller than 64×64 divisions, but we have no distortions.

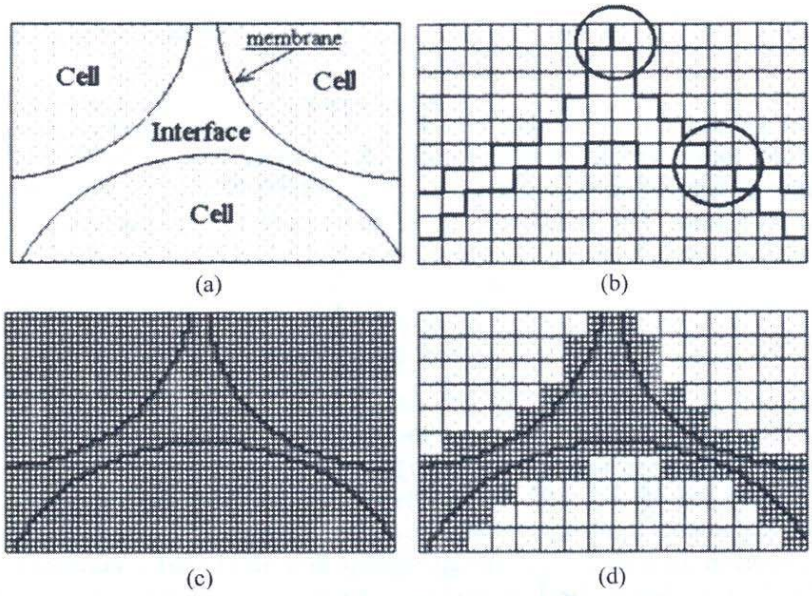

Figure 3. Biological system: (a) no discretization; (b) discretization with regular mesh of 16×16 division, circles indicate distortions; (c) regular mesh of 64×64, nodes total: 4,096; (d) regular mesh (16×16) with high-resolution definitions (node multiplier factor is 4), nodes total: 582.

The discretization length (Δx), used to calculate the time step, is the shortest dimension of mesh rectangles. The convergence rule is given by Eq. (4), from Ramos et al. (2003):

$$\Delta t < \frac{2\varepsilon/\sigma}{1 + 4(L_D/\Delta x)^2}, \tag{4}$$

where Δt are the time step, L_D is the Debye length, and ε and σ are the permittivity and conductivity of media, respectively.

System Description

This software is designed to work on IBM PC – Windows 32-bit platform. The program is written in Borland C^{++} Builder 5.0 Professional Edition. We suggest a minimum configuration of 1 GB RAM, 1.4 GHz processor, 20 G HD, screen resolution of 800 × 600 pixels, and Windows 98 SO.

The application uses Graphics32 library components (http://g32.org) to accelerate and optimize drawing on 32-bit device-independent bitmaps. Graphics32 is a set of functions, classes, components, and controls designed for high-performance graphics programing. It provides fast operations with pixels and graphic primitives. It was also required a library of visual components (SDL Software Development Lohninger, Austria, http://www.lohninger.com) which supports the display of 3-D surfaces and scientific graphs. The SDL Component Suite is comprised of routines and classes for computing in science and engineering.

User Interface

The main screen provides access to the plotting area, to draw the cell medium with representing cell membranes. In the left window, the user specifies the ionic environments. The ionic environment is formed by all ions that influence the electrical characteristics of a medium, like sodium. Each ion of an ionic environment is specified by: concentration [C/cm^3], mobility [cm^2.V^{-1}.s^{-1}], and electrical charge. Each ionic environment is associated to a color, with displays its spatial location within picture in the drawing area.

The drawing bar provides tools to draw the cell medium. A picture can be saved with BMP or VET format. The VET format is a binary file with the vectorial information of the picture. It is smaller than the correspondent BMP file, faster to open, and includes the discretization information.

In the discretization step, to each picture element we define the internal and external limits that set the boundaries of a high resolution discretization area. In the "Discretization Configuration" window, the user can check the nodes total and see a preview of the discretized medium.

The "Membrane Characteristics" window has inputs for two variables of electroporation equation. The membrane electropermeabilization model used assumes that all ionic transport should happen through the pores (Glaser et al., 1988; Ramos et al., 2004). After data input was completed, the user can execute the simulation. All input data are stored on independent files, but the PJC file (ASCII format) links all these files to the simulation.

The program has three graphic outputs: 2-D time domain, 3-D time domain, and 2-D frequency domain. In the 2-D time domain, we can observe the medium

current and electric field on the target cell, potential, and ionic currents of membrane.

The 3-D graphic presents: distribution of potential, current and electric field, the discretization of biologic medium as well as at every iteration (or time step). The user selects the iteration and the related graphic appear in the left.

The 3-D graphics may also be displayed as an animation (a sequence of graphics where the user can see the evolutions of the simulation results). In this movie the user indicates the initial and the last iteration and the iteration number between images.

The last graphic option is a semilog which presents the permittivity and conductivity values in the frequency domain. The user can save these results in the dielectric properties of tissue database.

Experiments

We present three numerical experiments: the first one is the analysis of a single cell, where we compare the simulation and theoretical results, skeletal muscle simulation, and a polygonal cell. The simulator utilizes the symmetry boundary condition to reduce time and memory requirement. Therefore, the analysis is realized in one quarter of biological systems.

In these simulations, we used the same electric properties for intra- and extracellular media given in Table 1. Membrane thickness is 10 nm and capacitance is $1\,\mu F/cm^2$. The internal and external limits of discretization are $1\,\mu m$. The membrane is considered intact.

Single cell. We studied effects of an applied electric field of 100 V/cm on single-cell membrane with radius $a = 50\,\mu m$. The analyzed region is $150 \times 87.5\,\mu m$, there are 92×50 divisions and the node multiplier is 5. The edge square of regular mesh is $D = 1.63\,\mu m$, and at the high resolution areas is $d = 0.33\,\mu m$. The number of nodes is 9,195. Time step is 0.3 ns and 20,000 iterations.

The analytical solution for the transmembrane voltage of a cylindrical membrane subjected to a uniform electric field, considering small membrane thickness and conductivity, from Ramos et al. (2003) and Stewart et al. (2005):

$$V_m = 2 \cdot E_o \cdot a \cdot \cos\theta \cdot \left(1 - e^{-t/\tau}\right), \tag{5}$$

Table 1
Medium electrical properties

Ions	Ionic density [$C.cm^{-3}$]	Ionic mobility* [$10^{-4}\,cm^2\,V^{-1}\,s^{-1}$]	Ionic diffusion coefficient* [$10^{-5}\,cm^2\,s^{-1}$]
Na^+	13.5	5.2	1.33
Cl^-	13.5	7.9	2.03

*Values in water for 298 K (Atkins, 1992; Barry and Lynch, 1991).

where a is the membrane radius, E_0 is the value of the uniform applied electric field applied, h is the membrane thickness, and the time constant is reduced to (6), from Schwan (1957):

$$\tau = a \cdot C_m \cdot \left(1/\sigma_i + 1/\sigma_o\right) \tag{6}$$

C_m is the capacitance per unit area of the membrane, σ_o and σ_i are the extra- and intracellular electrolyte conductivity, respectively.

Simulation results for skeletal muscle. We used a simplified 2-D model of a skeletal muscle tissue in a transversal plane. In this model, the skeletal muscle is only a group of very thin isolating membranes immersed in aqueous solution of ions.

Should symmetries be taken into account, analysis can be performed just in only a rectangular section (Fig. 4). Electric field as a step function of 100 V/cm was applied in the direction x. Cell radius is 50 μm and minimum distance among cells is 1 μm. The simulation parameter is similar to single cell. However, we analyzed more cells and the total nodes are 12,752.

The electrolyte permittivity is 78 (water contribution only). Membrane capacitance is 1 $\mu F.cm^{-2}$.

Polygonal cell. In the simulator discretization step, analysis of basic geometrical forms (e.g., circles, ellipses, and squares) is easy, with known equations. But, these forms are too simple to compare with real biological systems. So, we introduce here the polygonal form.

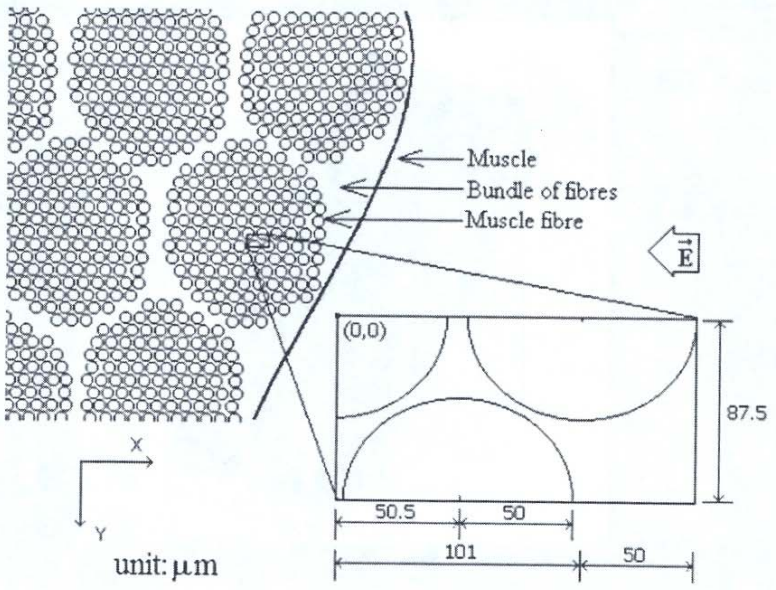

Figure 4. Simplified model of skeletal muscle in transversal plane. Cell radius is 50 μm and minimum distance among cells is 1 μm. The electrical field is in the direction x (Ramos et al., 2003).

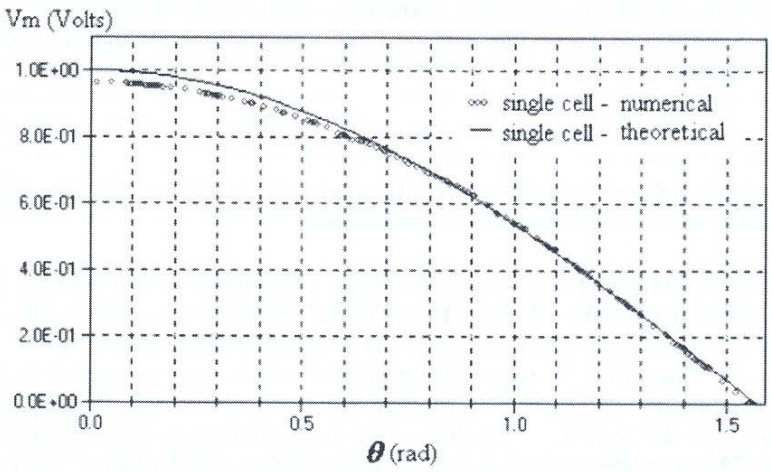

Figure 5. Theoretical and numerical behaviors of transmembrane potential on a single cell membrane in steady state. θ is the angle between electric field and position vector on the membrane.

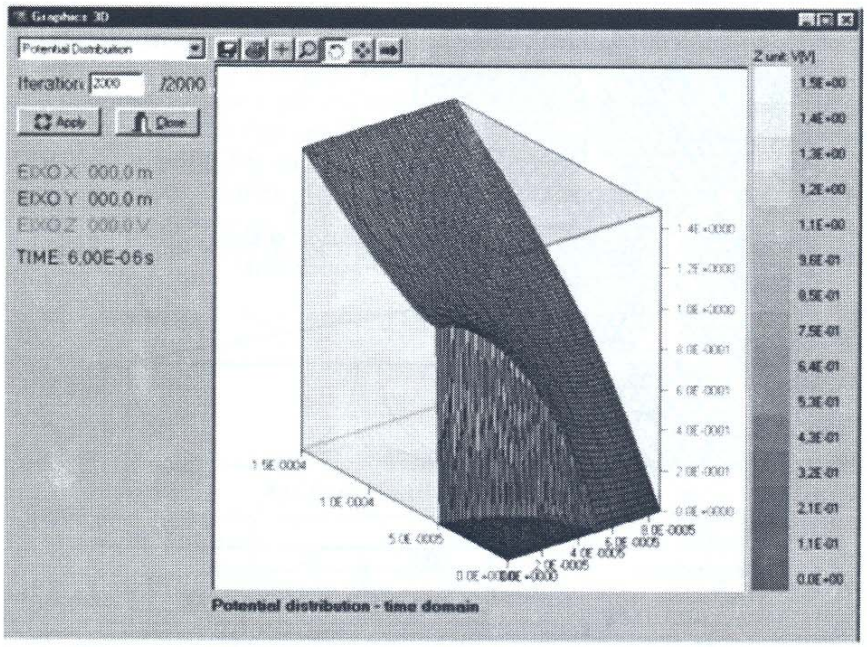

Figure 6. Potential distribution on single cell. The cosinusoidal decrease of transmembrane potential agrees with the theoretical curve.

The simulated area is $59 \times 40.8\,\mu m$, 30×40 divisions, node multiplier is 3, and total nodes are 1,968. Time step is 0.3 ns, total time $6\,\mu s$.

Results

Figure 5 shows the transmembrane potential (V_m) on the single-cell membrane in steady state. θ is the angle between electric field and position vector on the membrane. The potential distribution for a single cell is shown in Fig. 6. The cosinusoidal decrease of transmembrane potential agrees with Eqs. (4) and (5). The potential distribution on skeletal muscle in steady state is shown in Fig. 7. The potential within the cells are constant, and most of the potential drop happening in the membranes.

In Fig. 8, we show several shots of a animation. Firstly, the potential is linear in the biologic medium. After the electrical field application, the potential distribution change because the ions are moving. In the steady state, potential is constant inside the cells. Figure 9(a) presents the discretization of the polygonal form; nodes in high level representing the membranes. Figure 9(b) is the potential distribution, and Fig. 9(c) is the geometric pattern.

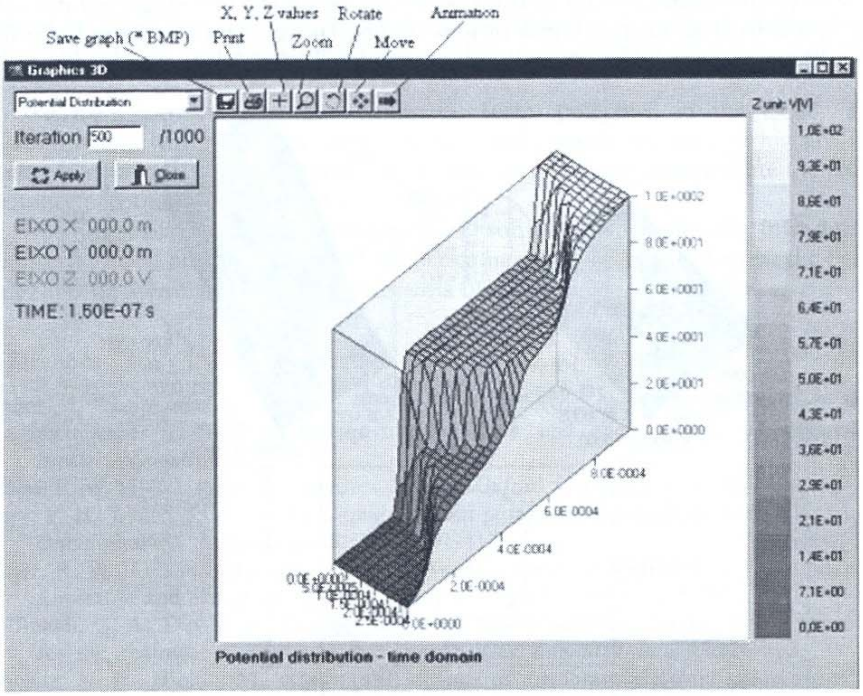

Figure 7. 3-D graphic of potential distribution $6\,\mu s$ after application of an electrical field step function of 100 V/cm x direction. X and Y axes describe the biologic medium orientation the potential is plotted on the Z axis.

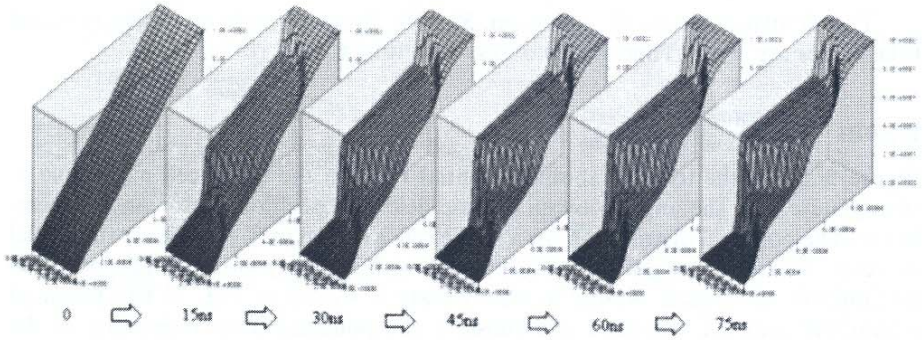

Figure 8. Screen shots of a graphic animation. The user can see the evolutions of the simulation results on space and time. First, the potential is linear in the biological medium, and after the electrical field application the distribution changes.

Discussion

Comparison between theoretical and numerical results for a single cell (Fig. 6) did not differ significantly: error of 3% at 0 rad. This result shows good overall agreement with numerical solution of cylindrical cell membranes using transport lattice method (Stewart et al., 2005).

The cosinusoidal decrease of transmembrane potential for a single cell indicates that at $\theta = 0$ rad an accumulation of ions occurs. However, at $\theta = 1.6$ rad, the flux

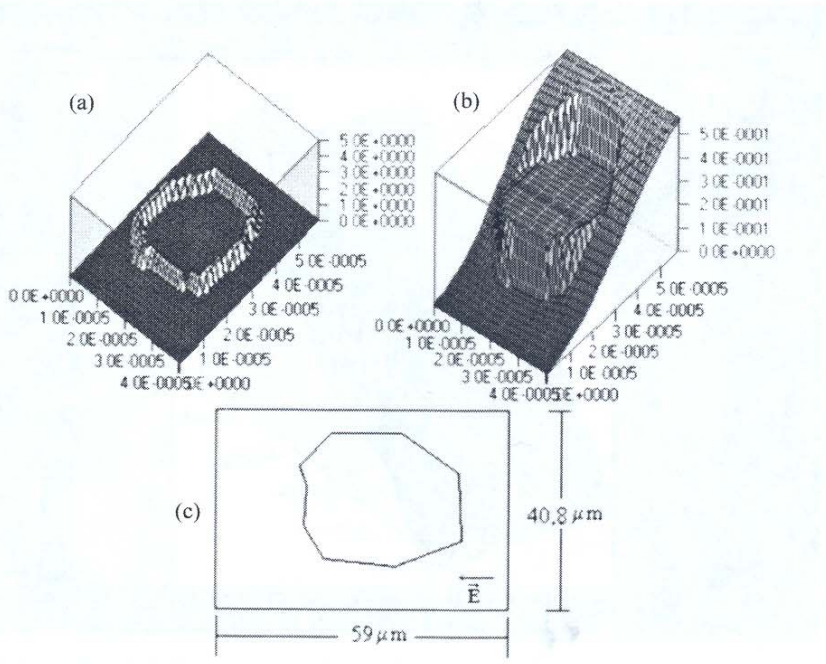

Figure 9. Polygonal form. (a) discretization, nodes in high level representing membranes; (b) potential distribution; (c) geometrical form of the polygonal cell.

of ions do not find any barrier. This V_m distribution agrees with experimental results of fluorescence microscope (Kinosita et al., 1992). V_m differences may govern the possibility of electroporation occurrence on the membrane (Weaver and Chizmadzhev, 1996).

In Fig. 9(b), the transmembrane potential at the polygon face parallel to the electric field does not decrease. This difference, between Figs. 9(b) and 6, indicates that the potential distribution depends on cell geometry. Moreover, experimental results demonstrate that the electroporation is a function of the cell shape and orientation (Valic et al., 2003).

The potential distribution of skeletal muscle model (Fig. 7) indicates that the electric field on the membranes (E_m) is higher than the applied field in the cell. When $E_m > 10^8$ V/m (Glaser et al., 1988), it enhances the reorientation of membrane phospholipid molecules, resulting in the covering of the inner surface of the pore. This shift from hydrophobic to hydrophilic pore allows ions to pass through the membrane (Abidor et al., 1979; Weaver and Mintzer, 1981).

The graphic animation sequential shots demonstrate rapid accumulation of charges in the membrane. This result corresponds with the induction of transmembrane potential in a sea urchin egg (Kinosita et al., 1992).

Simulator area is limited to $300 \times 300\,\mu$m. This area is enough for the majority of biological systems, as the simulator takes cell symmetry into account.

Conclusion

Results in Figs. 5, 7, and 9(b) stress the importance of potential distributions in biological cells to provide strong evidence for understanding the electroporation process.

We have introduced a new geometric form, polygons, in the ECM. The approximation with polygons shows better results when the real forms are not similar to circles, ellipses, or squares. With this work, we also demonstrate the ECM flexibility and the possibilities of the MDE.

Our future plans include: extension to 3-D software at the cell scale, introducing the discretization on the z-axis and high performance graphics, software at the tissue scale, and further mathematical refinements of the computational process.

References

Abidor, I. G., Arakelyan, L. V., et al. (1979). Electric breakdown of bilayer lipid membranes I. The main experimental facts and their qualitative discussion. *Bioelectrochemistry* 6:37–52.

Atkins, P. W. (1992). *Physical Chemistry*. Oxford: Oxford University Press, 837 pp.

Barry, P. H., Lynch, J. W. (1991). Liquid junction potentials and small cell effects in patch-clamp analysis. *J. Membrane Biol.* 121:101–117.

Glaser, R. W., Leikin, S. L., et al. (1988). Reversible electrical breakdown of lipid bilayers: formation and evolution of pores. *Biochem. Biophys. Acta* 940:275–287.

Hoffmann, G. A., Dev, S. B., Dimmer, S. (1996). Electroporation therapy: a new approach for the treatment of head and neck cancer. *IEEE Eng. Med. Biol.* 15:124–132.

Kinosita, K. Jr., Hibino, M., et al. (1992). Events of membrane electroporation visualized on a time scale from microsecond to seconds. In: Chang, D. C., Chassy, B. M., et al., eds. *Guide to Electroporation and Electrofusion*. San Diego: Academic Press, pp. 29–46.

Kinosita, K. Jr., Tsong, T. Y. (1977). Voltage-induced pore formation and hemolysis of human erythrocytes. *Proc. Natl. Acad. Sci. USA* 74:1923–1927.

Mir, L. M., Orlowski, S. (1999). Mechanisms of electrochemotherapy. *Adv. Drug Delivery Rev.* 35:107–118.

Neumann, E., Kakorin, S., Toensing, K. (2000). Principles of membrane electroporation and transport of macromolecules. In: Jaroszeski, M. J., Heller, R., Gilbert, R., eds. *Electrochemotherapy, Electrogenetherapy, and Transdermal Drug Delivery*. Totowa: Humana Press, pp. 1–35.

Ramos, A., Raizer, A., Marques, J. L. B. (2003). A new computational approach for electrical analysis of biological tissues. *Bioelectrochemistry* 5758:1–12.

Ramos, A., Suzuki, D. O. H., Marques, J. L. B. (2004). Numerical simulation of electroporation in spherical cells. *Artif. Org.* 28:357–361.

Schwan, H. P. (1957). Electric properties in tissue and cell suspensions. *Adv. Biol. Med. Phys.* 5:147–209.

Semrov, D., Miklavcic, D. (2000). Numerical modelling for in vivo electroporation. In: Jaroszeski, M. J., Heller, R., Gilbert, R., eds. *Electrochemotherapy, Electrogenetherapy, and Transdermal Drug Delivery*. Totowa: Humana Press, pp. 63–97.

Stewart, D. A. Jr., Gowrishankar, T. R., et al. (2005). Cylindrical cell membranes in uniform applied electric fields: validation of a transport lattice method. *IEEE Trans. Biomed. Eng.* 52:1643–1653.

Valencic, V., Krasna, A., et al. (1994). Numerical calculation and comparation of electromagnetic field parameters inside biological tissue. *Bioelectrochemistry* 35:115–119.

Valic, B., Golzio, M., et al. (2003). Effect of electric field induced transmembrane potential os spheroidalls: theory and experiment. *Eur. Biophys. J.* 32:519–528.

Weaver, J. C., Chizmadzhev, Y. A. (1996). Theory of electroporation: a review. *Bioelectrochemistry* 41:135–160.

Weaver, J. C., Mintzer, R. A. (1981). Decreased bilayer stability due to transmembrane potentials. *Phys. Lett.* 86A:57–59.